Excitation of Sr II lines in Eta Carinae

Bautista, M A; Gull, T R; Ishibashi, K; Hartman, Henrik; Davidson, K

Published in:
Monthly Notices of the Royal Astronomical Society

DOI:
10.1046/j.1365-8711.2002.05250.x

2002

Mon. Not. R. Astron. Soc. **331,** 875–879 (2002)

Excitation of Sr II lines in Eta Carinae

M. A. Bautista,[1★] T. R. Gull,[2] K. Ishibashi,[2†] H. Hartman[3] and K. Davidson[4]

[1]*Centro de Física, IVIC, Caracas 1020A, Venezuela*
[2]*Code 681, NASA Goddard Space Flight Center, Greenbelt MD, USA*
[3]*Department of Physics, Lund University, Lund, Sweden*
[4]*Astronomy Department, University of Minnesota, Minneapolis MN, USA*

Accepted 2001 December 3. Received 2001 December 3; in original form 2001 September 26

ABSTRACT

We study the nature of the peculiar [Sr II] and Sr II emission filament found in the ejecta of Eta Carinae. To this purpose we carry out *ab initio* calculations of radiative transition probabilities and electron impact excitation rate coefficients for Sr II. Then we build a multilevel model for the system which is used to investigate the physical condition of the filament and the nature of the observed allowed and forbidden Sr II optical emission. It is found that the observed spectrum is consistent with the lines being pumped by the continuum radiation field in a mostly neutral region with electron density near $10^7\,\mathrm{cm}^{-3}$. Under these conditions, the observed emission can be explained without the need for a large Sr overabundance.

Key words: atomic data – atomic processes – line: formation – stars: abundances – stars: individual: Eta Carinae.

1 INTRODUCTION

In 1999 February a series of STIS observation of Eta Car was made at a region about 1.5 arcsec north-west of the star. The spectrum showed two features at 6738.04 and 6867.85 Å which correspond to *forbidden lines of singly ionized strontium* ([Sr II]), Doppler-shifted by approximately $-100\,\mathrm{km\,s^{-1}}$. Other lines at about the same velocity come from [Cr II], [Ti II], [Mn II], [Co II], [Ni II], [Ca II], [Fe II] and [Fe I]. Curiously, no H I, He I, or [S II] lines were present. These spectra were followed up by observations with more complete spectral coverage on 2000 March 13. Then, the [Sr II] lines were again detected together with Sr II allowed emission at 4078 and 4216 Å (Zethson et al. 2001).

The observed [Sr II] lines come from transitions from the Sr^+ levels of the first excited configuration $4p^6 4d\ ^2D_{3/2,5/2}$ to ground level $4p^6 5s\ ^2S_{1/2}$. Resonant Sr II emission is produced by transitions from the excited multiplet $4p^6 5p\ ^2P^o_{1/2,3/2}$ to the ground level.

The cosmic abundance of strontium is $\log(N_{\mathrm{Sr}}/N_{\mathrm{H}}) = -9.08$ (Barklem & O'Mara 2000), i.e. lower than that of iron and nickel by factors of about 40 000 and 4000 respectively. Because of its low abundance, spectroscopic observations of strontium in objects other than the Sun are limited to a few objects enriched in s-process elements, like type II supernovae (SN1987A, Williams 1987; SN1995V, Fassia et al. 1998) and the Ba stars (e.g. Eggen 1972; Culver, Ianna & Franz 1977). The fact that [Sr II] lines were observed indicates that either strontium is locally overabundant in Eta Car by orders of magnitude or that unusual conditions exists in this region of the nebula.

^{88}Sr is produced by s-process neutron capture. It can become overabundant only under neutron-rich conditions during helium burning or later stages of stellar evolution. This is inconsistent with the evidence of CNO-cycle-processes ejecta. If the Sr overabundance is real, it must come from a putative compact companion of the observable central star that ejected the nebulosity.

We have carried out a systematic study of the excitation mechanisms of the Sr II ion that may explain the observed lines. We have calculated radiative transition rates and electron impact collision strengths for dipole allowed and forbidden transitions of Sr II. For these we use a 'state-of-the-art' method, namely the close coupling approximation with the Breit–Pauli **R**-matrix (BPRM) method. Then, we constructed a 12-level excitation balance model for Sr II including the effects of electron impact excitation and continuum fluorescence. This model is used to analyse the observed spectrum and to estimate the relative abundance of strontium in the observed region.

2 ATOMIC DATA FOR SR II

We have calculated atomic data (collisional excitation rates and radiative transition probabilities) for Sr II. The radiative transition probabilities and ion wavefunctions were obtained with the atomic structure code SUPERSTRUCTURE (Eissner, Jones & Nussbaumer 1974). The configuration interaction (CI) expansion employed includes the electron configurations $4s^2 4p^6 5s$, $4s^2 4p^6 4d$, $4s^2 4p^6 5p$ $4s^2 4p^6 6s$, $4s^2 4p^6 4f$, $4s^2 4p^6 5d$, $4s^2 4p^6 6p$, $4s^2 4p^5 5s^2$, $4s^2 4p^5 4d^2$,

★E-mail: mbautist@ivic.ve
†NAS/NRC Research Associate

Table 1. Energy levels in cm^{-1} of Sr^+.

Level	$E_{present}$	E_{exp} [a]
5s $^2S_{1/2}$	0.0	0.0
4d $^2D_{3/2}$	16133.	14555.9
4d $^2D_{5/2}$	16500.	14836.2
5p $^2P^o_{1/2}$	23315.	23715.2
5p $^2P^o_{3/2}$	24572.	24516.6
6s $^2S_{1/2}$	47116.	47736.5
5d $^2D_{3/2}$	52606.	53286.3
5d $^2D_{5/2}$	52731.	53373.0
6p $^2P^o_{1/2}$	54266.	55769.7
6p $^2P^o_{3/2}$	54587.	56057.9
4f $^2F^o_{5/2}$	59922.	60991.7
4f $^2F^o_{7/2}$	59924.	60991.7

[a]Moore (1983)

Table 2. f-values for electric dipole transitions of Sr^+.

Transition	$f_{present}$	f_{exp} [a]	f_{exp} [b]
5p $^2P^o_{3/2}$–5s $^2S_{1/2}$	0.75	0.71 ± 0.03	0.72 ± 0.01
5p $^2P^o_{1/2}$–5s $^2S_{1/2}$	0.36	0.34 ± 0.015	0.36 ± 0.01
5p $^2P^o_{3/2}$–4d $^2D_{5/2}$	0.084	0.096 ± 0.02	
5p $^2P^o_{3/2}$–4d $^2D_{3/2}$	0.015	0.016 ± 0.03	
5p $^2P^o_{1/2}$–4d $^2D_{3/2}$	0.062	0.084 ± 0.015	

[a]Gallagher (1967)
[b]Pinnington, Berends & Lumsden (1995)

$4s^24p^55p^2$, $4s^24p^56s^2$, $4s^24p^54f^2$, $4s^24p^55d^2$, $4s^24p^56p^2$, $4s^24p^55s4d$, $4s^24p^55s5p$, $4s^24p^55s6s$ $4s^24p^55s4f$ $4s^24p^55s5d$, $4s^24p^55s6p$, $4s^24p^54d5p$, $4s^24p^54d6s$, $4s^24p^54d4f$ $4s^24p^54d5d$, $4s^24p^54d6p$, $4s^24p^55p6s$, $4s^24p^55p4f$ $4s^24p^55p5d$, $4s^24p^55p6p$, $4s4p^65s^2$, $4s4p^65s4d$, $4s4p^65s5p$ $4s4p^65s6s$, $4s4p^65s4f$, $4s4p^65s5d$, $4s4p^65s6p$, $4s4p^64d^2$, $4s4p^64d5p$ $4s4p^64d6s$, $4s4p^64d4f$, $4s4p^64d5d$, $4s4p^64d6p$. This large expansion yields eigenenergies that agree within 2 per cent for most levels, except for the 4d ^2D levels which differ from experiment by nearly 11 per cent (see Table 1). The f-values obtained with this expansion also agree well with experimental determinations, within ∼10 per cent for all but one transition (see Table 2).

We have computed electron impact collision strengths for transitions among the 12 lowest energy levels of Sr II that belong to the configurations $4p^65s$, $4p^64d$, $4p^65p$, $4p^66s$, $4p^64f$, $4p^65d$ and $4p^66p$. We employ the Breit–Pauli **R**-matrix method (BPRM) and the set of codes developed in the framework of the IRON Project (Hummer et al. 1993). Schoning & Butler (1998) showed that the Breit–Pauli approximation accounts reasonably well for the relativistic effects in elements as heavy as xenon ($Z = 54$) and barium ($Z = 56$), for which BPRM results agree within 20 per cent with the results of the fully relativistic Dirac **R**-matrix theory. Thus, the BPRM method is expected to be accurate for the case of strontium ($Z = 38$). The calculated collision strengths include important contributions from near threshold autoionizing resonances. Fig. 1 shows the collision strengths for some of the dominant transitions.

Effective collision strengths and excitation rates were obtained by integrating the collision strengths over a Maxwellian distribution of electron velocities for various temperatures between 5 000 and 20 000 K.

3 EXCITATION OF SR II

We build a 12-level excitation equilibrium model for Sr II. which considers both electron impact excitation and continuum fluorescence excitation (see Fig. 2). A model of this size is enough to account for collisionally excited emission because at the temperatures that Sr II can exist ($< 10^4$ K) only the ground state and the first two excited configurations are significantly populated. The additional higher excitation levels in our model account for the most important photoexcitation channels from the ground level. If more levels were included in our models they would tend to increase the fluorescence excitation efficiency, although it has been shown that individual levels contributions decreases rapidly with the level excitation (Bautista, Peng & Pradhan 1996). We assume that the radiation field density, U_ν, at photon energies below the Lyman ionization limit (13.6 eV) can be approximated by a blackbody with temperature T_R times a geometrical dilution factor w, i.e.

$$\frac{c^3 U_\nu}{8\pi h\nu^3} = \frac{w}{\exp(h\nu/kT_R) - 1}. \quad (1)$$

For the present calculations we try various blackbody temperatures between 25 000 and 60 000 K and dilution factors looking for the best match to the observed spectra.

Fig. 2 presents the adopted energy level diagram for Sr^+. The diagram shows that photo-pumping of the λλ6740.25 and 6870.07-Å levels may occur by resonant photo-excitation from the ground $4p^65s$ ^2S level to the $4p^65p$ $^2P^o$ levels followed by dipole-allowed de-excitation to the $4p^64d$ ^2D levels. Direct inspection of radiative transition rates shows that approximately 6 per cent of all photoabsorptions to the $3p^65p$ $^2P^o$ levels will end up into the $3p^64d$ ^2D levels, while the remaining ∼94 per cent will

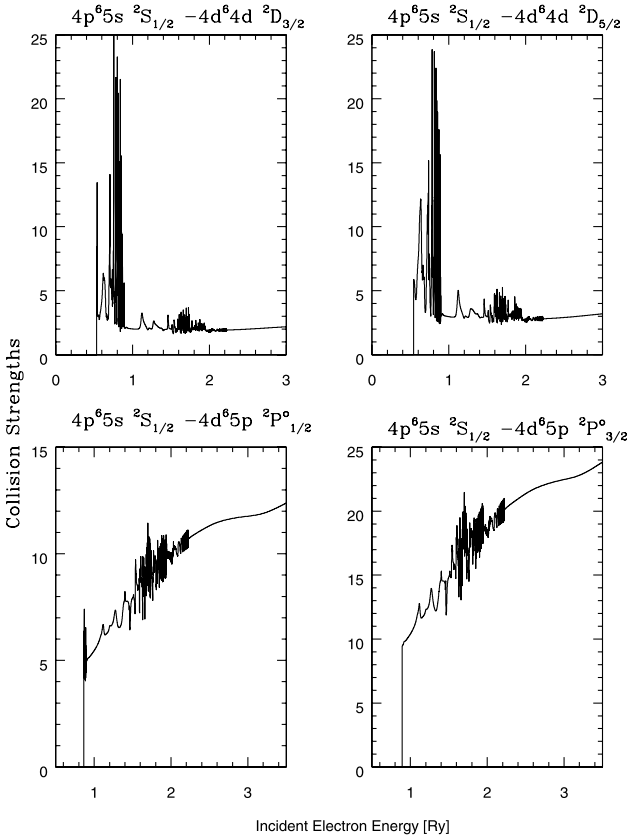

Figure 1. Sample of collision strengths versus incident electron energy.

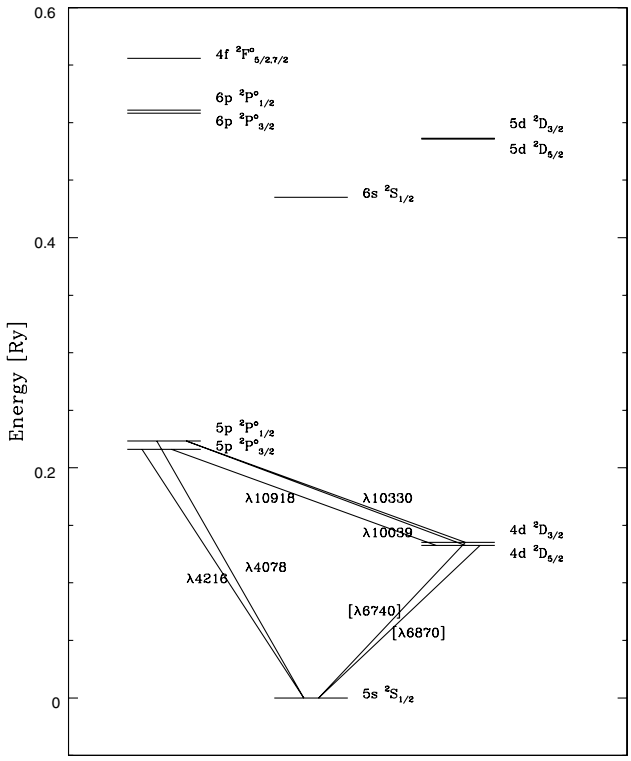

Figure 2. Energy diagram of Sr^+.

return back down to the ground level. Photoabsorption to other $^2P^o$ levels may also contribute to the pumping.

Fig. 3 presents the line emissivity per ion of [Sr II] λ6740.3 ($4p^6 5s\ ^2S_{1/2} - 4p^6 4d\ ^2D_{5/2}$) versus N_e for a blackbody temperature of 40 000 K and four values of the dilution factor, $w = 0$ (no fluorescence), 10^{-11}, 10^{-9} and 10^{-7}. It is seen that the intensity of the [Sr II] lines can be enhanced by up to several orders of magnitude by continuum fluorescence.

An upper bound for the geometrical dilution factor of 1.4×10^{-9} is estimated from the observed projected distance from the filament to the central star. The actual value of the dilution factor may be smaller than this depending on the projection angle for the vector that connects the central star to the filament. In addition, a small fraction of photons from the central source are likely to be absorbed by dust. On the other hand, the intensity of the radiation field also depends on the effective temperature of the source, in such a way that if the actual temperature were underestimated the effect on the spectrum would be compensated by increasing the dilution factor, and vice versa.

4 PHYSICAL CONDITIONS AND THE STRONTIUM ABUNDANCE

Line emissivity ratios are also affected by fluorescence. The line intensity ratio $I(\lambda6740)/I(\lambda6870)$ in Fig. 4(a) can be used for electron density diagnostics in the range $\sim 10^6$–$10^9\,\mathrm{cm}^{-3}$. At low densities and in the presence of continuum fluorescence excitation the ratio becomes smaller than under pure collisional excitation. As N_e increases collisional excitation dominates and all the curves for different dilution factors merge. The observed line ratio of

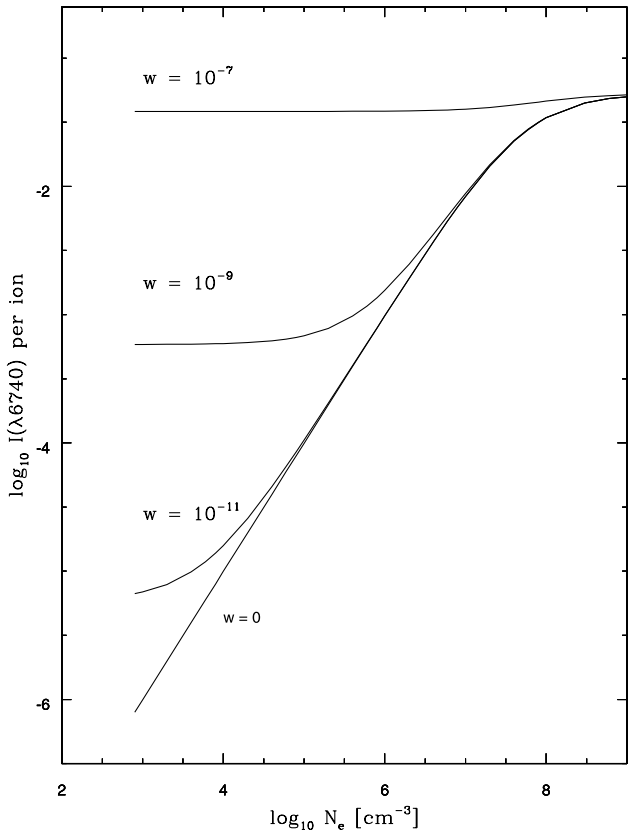

Figure 3. The intensity of the [Sr II] λ6740 per Sr^+ ion versus electron density for various values of the dilution factor.

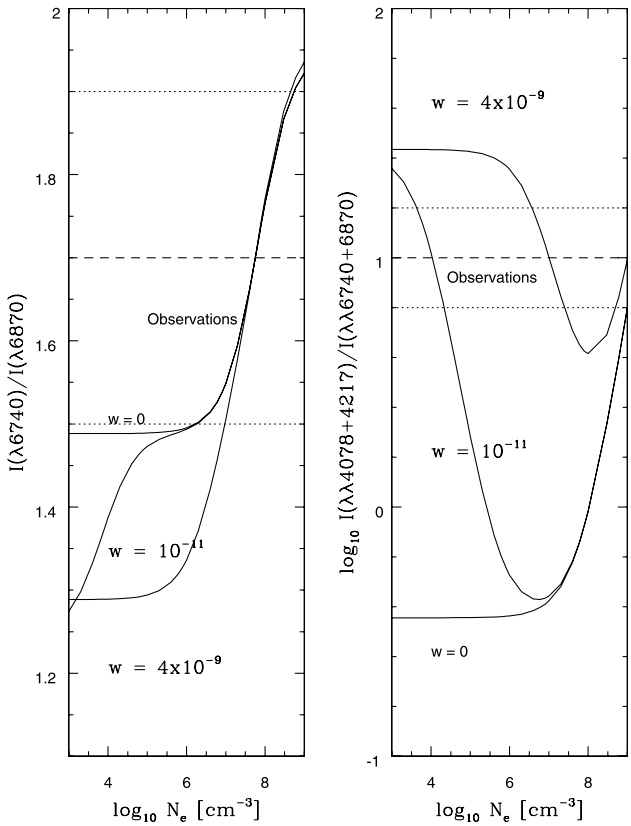

Figure 4. Line emissivity ratios versus electron density for various values of the dilution factor.

1.7 ± 0.2 (consistently obtained from two different observations in 1999 and 2000) is consistent with an electron density of the order of $10^7\,\mathrm{cm}^{-3}$. Electron densities much lower than $10^7\,\mathrm{cm}^{-3}$ seem ruled out, especially for the case of a dilution factor near 10^{-9}.

Another interesting ratio is that of resonant to forbidden lines, $\log_{10}[I(\lambda\lambda 4078+4217)/I(\lambda\lambda 6740+6870)]$ versus N_e, shown in Fig. 4(b). Under low density conditions this ratio is enhanced by up to several orders of magnitude by continuum fluorescence and the magnitude of the enhancement is quite sensitive to values of the dilution factor and the shape of the radiation field. The observed value, corrected for extinction, is $\log_{10}[I(\lambda\lambda 4078+4217)/I(\lambda\lambda 6740+6870)] = 1.0 \pm 0.2$, where most of the error comes from the uncertainty in the visual extinction (A_V), which is expected to be around 2 magnitudes for a standard extinction curve. In this case the observed ratio lies above any possible value for pure collisional excitation. On the other hand, the observed ratio is in reasonable agreement with $N_\mathrm{e} \approx 10^7\,\mathrm{cm}^{-3}$ if $w = 4 \times 10^{-9}$.

These two line ratios, between forbidden lines and of allowed to forbidden lines, can be used together to constrain the range of possible values of the dilution factor (w) for every blackbody temperature. Fig. 5 shows the maximum and minimum dilution factors that can reproduce the observed spectrum, given the observational errors, for any blackbody temperature between 25 000 and 60 000 K. This range of dilution factors that match the spectrum is consistent with the value of around 1.4×10^{-9}, based on purely geometrical grounds, for a radiation field temperature of about 45 000 K or hotter.

In addition to relatively high electron densities and fluorescence excitation, the strontium region must have particular ionization conditions. The energy required to ionize Sr into Sr^+ is 5.7 eV and the energy to ionize Sr^+ into Sr^{2+} is 11.0 eV. The latter is comparable to the energy of 10.4 eV needed to produce S^+ and lower than the ionization energy of H (13.6 eV). Thus, Sr^+ may only survive in regions of very low ionization where even S and H are mostly neutral. On the other hand, Sr^+ may coexist in part with Fe^+ and Ni^+ which only need 7.6 and 7.9 eV to be formed.

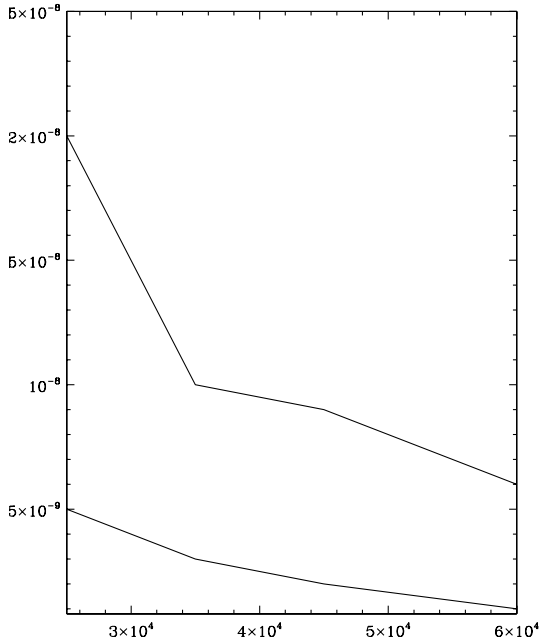

Figure 5. Range of allowed values for the dilution factor for different blackbody temperatures of the continuum fluorescence radiation field.

Assuming $N_\mathrm{e} = 10^7\,\mathrm{cm}^{-3}$ and considering the whole range of blackbody temperatures and dilution factors consistent with the Sr II spectrum we find an abundance ratio $N(\mathrm{Ni}^+)/N(\mathrm{Sr}^+) = 140 \pm 70$. The error in this estimate includes uncertainty in the extinction correction and the scatter in line emissivities for different allowed temperatures and dilution factors. Two things are to be noted about this calculation. First, unlike the [Sr II] emission, the [Ni II] lines are composed of several components at different radial velocities. Thus, we consider only the [Ni II] line component at the same velocity as the [Sr II] emission. Secondly, the [Ni II] emission is also sensitive to continuum fluorescence (Lucy 1995; Bautista et al. 1996). For the present calculation we use the models for Ni II of Bautista et al. but include improved collisional excitation rates (Bautista, in preparation).

Only neutral and singly ionized ions are present in the spectra. There is evidence for a significant fraction of neutral iron, and consequently of nickel since both ions are tied to each other by charge exchange. On the other hand, the ionization of Sr should be higher than that of Ni because of the significantly lower ionization potential of Sr. Thus, $N(\mathrm{Ni})/N(\mathrm{Sr}) > N(\mathrm{Ni}^+)/N(\mathrm{Sr}^+) \approx 140$. The remaining factor of enhancement of Sr with respect to Ni, not greater than a decade, may be explained in terms of differences in the fractions of depletion of both elements. Sr is a refractory element, the atomic structure and temperatures of fusion and sublimation of which are much lower than those of Fe and Ni, similar to those of Ca (e.g. Irvine & Knacke 1989). Then, it is likely that the depletion of Fe and Ni is higher than that of Sr in the ionized nebula. Furthermore, the observed Sr II emission may be explained without the need for a large overabundance of strontium.

5 DISCUSSION

We have calculated radiative transition rates and electron impact collision strengths for dipole allowed and forbidden transitions of Sr II. These data were used to study the excitation mechanisms of optical allowed and forbidden Sr II lines. It is shown that the observed forbidden and allowed Sr II emission can be explained by a combination of continuum fluorescence and high electron density ($\sim 10^7\,\mathrm{cm}^{-3}$) in a predominantly neutral region.

It is likely that the Sr II emission comes from a region illuminated by low-energy radiation but shielded from radiation with energy ~ 10 eV and higher. If this scenario is correct it leads to the next question: How is such a low ionization region sustained? Or in other words: What continuum radiation spectrum and conditions within the filament are required to sustain a sufficiently large observable region? Partially ionized regions around a H II region are typically quite thin owing to high optical depth to the ionizing Lyman continuum radiation and, subsequently, a rapid drop in the temperature. On the other hand, active galactic nuclei (AGNs) can have extensive partially ionized zones because of penetrating X-rays from the non-thermal continuum source and high gas densities to maintain substantial population in the $n = 2$ levels of hydrogen which are then photoionized by Balmer continuum radiation. This latter mechanism seems unlikely to occur in the strontium filament, since no hydrogen recombination emission is observed at all. Furthermore, investigating the nature of the strontium filament of Eta Car is of general importance in the understanding of partially-ionized zones in photoionized nebulae.

Further observational and theoretical work is under way trying to constrain better the radiation field illuminating the filament and the ionization mechanisms. This work should provide better

estimates of the strontium abundance in the filament and explain the mechanisms that sustain such a low ionization region.

REFERENCES

Barklem P. S., O'Mara B. J., 2000, MNRAS, 311, 535
Bautista M. A., Peng J., Pradhan A. K., 1996, ApJ, 460, 372
Culver R. B., Ianna P. A., Franz O. G., 1977, PASP, 89, 397
Eggen O. J., 1972, MNRAS, 159, 403
Eissner W., Jones M., Nussbaumer H., 1974, Comput. Phys. Commun., 8, 270
Fassia A., Meikle W. P. S., Geballe T. R., Walton N. A., Pollacco D. L., Rutten R. G. M., Tinney C., 1998, MNRAS, 299, 150
Gallagher A., 1967, Phys. Rev., 157, 157
Hummer D. G., Berrington K. A., Eissner W., Pradhan A. K., Saraph H. E., Tully J. A., 1993, A&A, 279, 298
Irvine W. M., Knacke R. F., 1989, in Atreya S. K., Pollak J. B., Matthews M. S., eds, Origin and Evolution of Planetary and Satellite Atmospheres. Univ. Arizona Press, Tucson, pp. 3–34
Lucy L. B., 1995, A&A, 294, 555
Moore C. E., 1983, Selected tables of atomic spectra, NSRDS-NBS. National Bureau of Standards, Washington DC
Pinnington E. H., Berends R. W., Lumsden M., 1995, J. Phys. B: Atom. Mol. Op. Phys., 28, 2095
Schoning T., Butler K., 1998, A&A, 128, 581
Williams R. E., 1987, ApJ, 320, L117
Zethson T., Gull T. R., Hartman H., Johansson S., Davidson K., Ishibashi K., 2001, AJ, 122, 322

This paper has been typeset from a TEX/LATEX file prepared by the author.